



# The New EXor Outburst of ESO-H $\alpha$ 99 Observed by *Gaia* ATLAS and *TESS*

Klaus W. Hodapp<sup>1</sup> , Bo Reipurth<sup>1</sup> , Bertil Pettersson<sup>2</sup>, John Tonry<sup>3</sup> , Larry Denneau<sup>3</sup>, Patrick J. Valley<sup>4</sup>, Benjamin J. Shappee<sup>3</sup> , James D. Armstrong<sup>5</sup>, Michael S. Connelley<sup>1</sup>, C. S. Kochanek<sup>4</sup> , Michael Fausnaugh<sup>6</sup> , Rolf Chini<sup>7,8</sup>, Martin Haas<sup>7</sup>, and Catalina Sobrino Figaredo<sup>9</sup>

<sup>1</sup> University of Hawaii, Institute for Astronomy, 640 N. Aohoku Place, Hilo, HI 96720, USA; [hodapp@ifa.hawaii.edu](mailto:hodapp@ifa.hawaii.edu)

<sup>2</sup> Department of Physics and Astronomy, Uppsala University, Box 516, SE-751 20 Uppsala, Sweden

<sup>3</sup> University of Hawaii, Institute for Astronomy, 2680 Woodlawn Drive, Honolulu, HI 96822, USA

<sup>4</sup> Department of Astronomy, The Ohio State University, 140 West 18th Avenue, Columbus OH 43210-1173, USA

<sup>5</sup> University of Hawaii, Institute for Astronomy, 34 Ohia Ku Street, Pukalani, HI 96768, USA

<sup>6</sup> MIT Kavli Institute for Space and Astrophysics Research, 77 Massachusetts Avenue, 37-241, Cambridge, MA 02139, USA

<sup>7</sup> Astronomisches Institut, Ruhr-Universität Bochum, Universitätsstraße 150, D-44801 Bochum, Germany

<sup>8</sup> Instituto de Astronomia, Universidad Católica del Norte, Avenida Angamos 0610, Antofagasta, Chile

<sup>9</sup> Astronomisches Institut, Ruhr-Universität Bochum, Universitätsstraße 150, D-44801 Bochum, Germany

Received 2019 July 1; revised 2019 September 16; accepted 2019 September 22; published 2019 November 20

## Abstract

We report photometry and spectroscopy of the outburst of the young stellar object ESO-H $\alpha$ 99. The outburst was first noticed in *Gaia* alert Gaia18dvc and later by the Asteroid Terrestrial-impact Last Alert System (ATLAS). We have established the outburst light curve with archival ATLAS orange filter photometry, *Gaia* data, new *V*-band photometry, and *J*, *H*, and *K<sub>s</sub>* photometry from the Infrared Imaging System (IRIS) and the United Kingdom Infrared Telescope (UKIRT). The brightness has fluctuated several times near the light curve maximum. The *Transiting Exoplanet Survey Satellite* (*TESS*) satellite observed ESO-H $\alpha$  99 with high cadence during one of these minor minima and found brightness fluctuations on timescales of days and hours. Imaging with UKIRT shows the outline of an outflow cavity, and we find one knot of H $_2$  1 – 0 *S*(1) emission, now named MHO 1520, on the symmetry axis of this nebula, indicating recent collimated outflow activity from ESO-H $\alpha$  99. Its pre-outburst SED shows a flat far-infrared spectrum, confirming its early evolutionary state and its similarity to other deeply embedded objects in the broader EXor class. The pre-outburst luminosity is 34  $L_{\odot}$ , a much higher luminosity than typical EXors, indicating that ESO-H $\alpha$  99 may be a star of intermediate mass. Infrared and optical spectroscopy show a rich emission-line spectrum, including H I lines, strong red Ca II emission, as well as infrared CO bandhead emission, all characteristic EXors in the broadest sense. Comparison of the present spectra with an optical spectrum obtained in 1993, presumably in the quiescent state of the object, shows that during the present outburst the continuum component of the spectrum has increased notably more than the emission lines. The H $\alpha$  equivalent width during the outburst is down to one-half of its 1993 level, and shock-excited emission lines are much less prominent.

*Unified Astronomy Thesaurus concepts:* Eruptive variable stars (476); Young stellar objects (1834); T Tauri stars (1681); Infrared photometry (792); Flash spectra (541); Stellar jets (1607)

## 1. Introduction

Young stellar objects (YSOs) in spectral energy distribution (SED) classes I and II, i.e., stars in their late accretion phase, often show substantial variability due to instabilities in the accretion process. The accretion characteristics of young stars have recently been reviewed by Hartmann et al. (2016) and we follow their general line of discussion and the references therein.

Traditionally, the photometric outbursts caused by increased accretion rates were divided by Herbig (1977) into two classes: FU Orionis objects (FUor) and EX Lupi objects (EXor). The outburst amplitude is similar for both classes, but the FUor outbursts last for decades to centuries, while EXor outbursts last from months to maybe a few years.

The first known outburst of a YSO, FU Orionis, still remains the most substantial of these accretion instability events, having hardly declined in brightness from its maximum as first discussed by Herbig (1977). For a recent comparison of FUor-type light curves see Hillenbrand et al. (2019), who compare the recently discovered FUor PTF14jg with the classical examples, and the comprehensive review of eruptive YSOs by Audard et al. (2014). EXors, on the other hand, are typically

repetitive on timescales of a few years to decades, as illustrated in the case of the deeply embedded EXor V1647 Ori in a series of papers by Reipurth & Aspin (2004), Aspin et al. (2006, 2008, 2009, 2009), Aspin & Reipurth (2009), and Aspin (2011b), and more broadly reviewed by Audard et al. (2014).

While most EXors have shown repeated outbursts on timescales of many years to decades, repetitive accretion instabilities on timescales from weeks down to hours have been found in many other YSOs, e.g., the Young Stellar Object Variability (YSOVAR) studies of NGC 2264 by Cody et al. (2014) and Stauffer et al. (2014) and the *Kepler-2* variability study by Cody et al. (2017). In many young stars still surrounded by substantial disks, both accretion instabilities (outbursts) and extinction variations (dipper events) are observed, and in some cases it can be difficult to discern which of the two mechanisms dominates.

The two classical types of YSO outburst are also distinct spectroscopically. EXors show a rich emission-line spectrum probably produced in optically thin funnel flows in a magnetospheric accretion scenario and veiling of photospheric absorption lines by an UV and optical continuum produced in

high-temperature shocks. The more substantial FUor outbursts show a low-gravity absorption line spectrum reminiscent of a supergiant photosphere thought to be caused by a self-luminous optically thick accretion disk in a scenario where the accretion rate from that disk has overwhelmed the stellar magnetosphere and pushed it back to the stellar surface (Hartmann et al. 2016). However, FUor spectra are distinct from those of supergiant photospheres with their characteristic shift of the spectral type with wavelength. Spectra in the near-infrared are classified as a later (cooler) spectral type than the optical spectra.

The original prototypical objects FU Orionis and EX Lupi used by Herbig (1977) were discovered using photographic methods best suited for bright and blue objects. As more and more YSO outbursts have been observed thanks to better all-sky monitoring and infrared surveys these newer objects begin to fill a continuum of light curve characteristics such as amplitude, rise time, and rate of decline. Also, some YSO outbursts defy classification into the FUor or EXor types, either because their outburst duration or spectrum falls between that of the classical classes, or because the spectrum defies classification. Examples of such outbursts with intermediate characteristics between classical FUor and EXor outbursts are V1647 Ori (Aspin 2011b, and references therein), ASASSN-13db (Sicilia-Aguilar et al. 2017), and PV Cep (Kun et al. 2011; Lorenzetti et al. 2011, 2015). Such outbursts with intermediate characteristics, in particular more deeply embedded than EX Lupi itself, being associated with reflection nebulosity and outflow features, and being more luminous than EX Lupi, have been called Newest EXors by Lorenzetti et al. (2012) and MNors by Contreras Peña et al. (2017a, 2017b). However, even more extreme transition objects exist that call into question whether we know enough about the properties of young eruptive variables to properly define new classes of this phenomenon.

For example, the deeply embedded YSO SVS 13 = V512 Per that shows an emission-line spectrum was originally listed as an EXor (Eisloffel et al. 1991; Aspin & Sandell 1994). However, the light curve differs from that of typical EXors, since it has not returned to the pre-outburst brightness 25 yr after the outburst (Hodapp & Chini 2014). As an extreme case one outburst with a duration of decades and with a completely line-free dust continuum spectrum, OO Ser, was observed by Hodapp et al. (1996, 2012) and originally labeled as a deeply embedded outburst star (DEOS).

The total number of known YSO outburst objects is still quite small, at most a few dozen objects of the FUor, EXor, and intermediate cases combined, even though the discovery rate has been improving in recent years thanks to several all-sky and infrared monitoring projects. Every newly discovered object therefore deserves careful analysis. We report here on the preliminary characterization of ESO-H $\alpha$  99, also listed as IRAS08370–4030, located at 08:38:55.17–40:41:17.34 (J2000.0) in the Vela Molecular Ridge (VMR), whose outburst was first noted by *Gaia* alert Gaia18dvz on 2018 December 19.<sup>10</sup>

## 2. ESO-H $\alpha$ 99: Context and Pre-outburst Properties

### 2.1. Context

The VMR is a massive molecular cloud complex straddling the border of Vela and Puppis along the Galactic plane between Galactic longitudes 259° and 272°. It was first noted by Dame et al. (1987) and May et al. (1988). Murphy & May (1991) identified four separate clouds, which they called A, B, C, and D. A detailed CO survey of the entire VMR was presented by Yamaguchi et al. (1999). The distance to the VMR is poorly known, and over the years numerous estimates have been made to individual regions in the VMR, ranging from 0.7 kpc to 2 kpc (Pettersson 2008). The *Gaia* DR2 parallax of ESO-H $\alpha$  99 is  $1.2518 \pm 0.3176$  mas ( $\approx 800 \pm 300$  pc), not a very precise value due to the faintness of this object. Here we adopt a newly determined distance to VMR-D of  $1007 \pm 30$  pc determined by B. Pettersson and B. Reipurth (2019, in preparation) based on *Gaia* DR2 parallax data of all H $\alpha$  emitting stars in this region. This new distance measurement places the VMR between the foreground Gum Nebula and the background Carina–Sagittarius arm (Pettersson 2008), producing a complex line of sight. In particular it should be noted that the VMR is seen behind the OB association Trumpler 10. Star formation is abundant all along the VMR as was pointed out by Liseau et al. (1992), Giannini et al. (2007), and Massi et al. (2007).

The northwestern part of the ridge is VMR-D, which is dominated by three H II regions, RCW 27, 32, and 33 (Rodgers et al. 1960). All of these regions are actively forming stars, which have been studied at multiple wavelengths, e.g., by Strafella et al. (2010, 2015, and references therein). It appears that RCW 27 is a particularly fertile star-forming region. Pettersson & Reipurth (1994) carried out a large survey for H $\alpha$  emission stars toward RCW 27, 32, and 33, many of which have subsequently been identified as T Tauri stars, e.g., by Prisinzano et al. (2018). One of these young emission-line stars is ESO-H $\alpha$  99, the object of this paper. ESO-H $\alpha$  99 was detected by *IRAS* and is the dominant flux source of *IRAS* 08370–4030. This star is partly embedded in the dense high-extinction cloud Sandqvist 1, which is seen against the RCW 27 H II region (Sandqvist & Lindroos 1976). Prominent bright rims are seen in the infrared *Spitzer* image (Figure 1, bottom panel), which are likely excited by the OB star in RCW 27. In contrast, no bright rims are seen in the red optical image (Figure 1 top panel) suggesting that we are seeing the Sandqvist 1 cloud from the unilluminated back side.

### 2.2. Pre-outburst SED

Figure 2 shows the SED of ESO-H $\alpha$  99 based on ground-based and space-based survey data obtained from VizieR. The infrared and far-infrared data are from the compilation of catalog data by Abrahamyan et al. (2015, and references therein) and include data from the *Wide-field Infrared Survey Explorer*, *Midcourse Space Experiment (MSX)*, *AKARI*, and *IRAS*. The Two Micron All Sky Survey (2MASS) data are from the point-source catalog (Skrutskie et al. 2006). The photographic data points (DSS) are from the guide-star catalog of Lasker et al. (2008). *Gaia* data are from data release DR 1 and DR 2 (Gaia Collaboration et al. 2016, 2018). Other optical data are from Prisinzano et al. (2018, and references therein). Note that the SED in Figure 2 does not include the *IRAS* 100  $\mu$ m data point because of the low spatial resolution of that data point

<sup>10</sup> <http://gsaweb.ast.cam.ac.uk/alerts/alert/Gaia18dvz/>

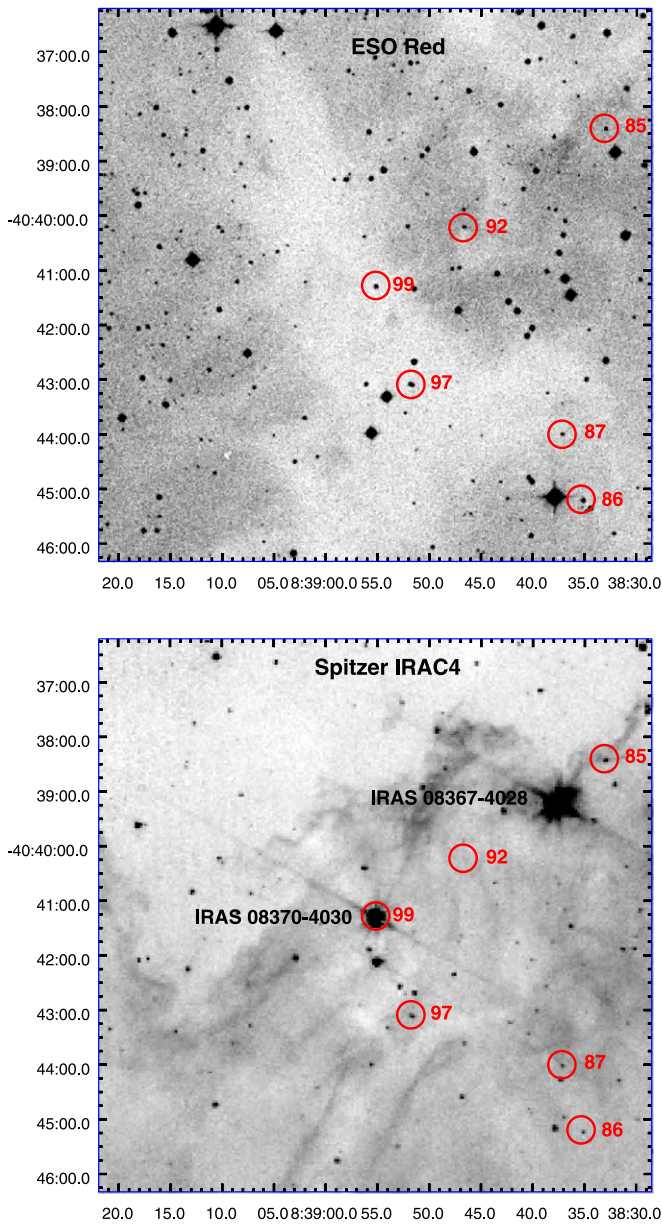


**Figure 1.** Overview of the region containing ESO-H $\alpha$  99 at optical (ESO Red) and infrared (*Spitzer* IRAC4) wavelengths. The features of the foreground extinction visible in the red image is uncorrelated to the polycyclic aromatic hydrocarbon (PAH) emission dominating the IRAC4 image, illustrating the complicated line of sight. ESO-H $\alpha$  stars are marked and numbered. ESO-H $\alpha$  99 and IRAS 08370–4030 are the same object, with the caveat of possible beam contamination in the *IRAS* data.

and likely possible contamination from neighboring far-infrared sources, the closest bright one being IRAS 08367–4028.

The most important unsubstantiated assumption in this SED is that all the measurements refer to the quiescent state of the object. We do not have a well-measured light curve of this object prior to the start of regular monitoring by *Gaia* and ATLAS to place any of the SED data points into the context of a light curve. It is quite possible that the substantial scatter in the flux measurements at optical wavelengths, well above the errors indicated in Figure 2, is due to variability. The SED is a typical flat-spectrum distribution (Greene et al. 1994). The flat part of the SED extends from the near-infrared *K* band at

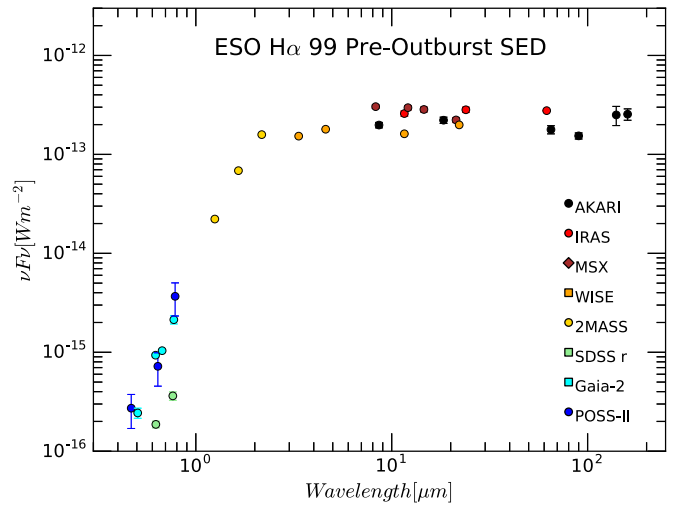


**Figure 2.** Pre-outburst SED of ESO-H $\alpha$  99 from catalog data available in the VizieR database. Individual references are in the text. The SED longward of the *K<sub>s</sub>* band is remarkably flat.

2.15  $\mu\text{m}$  out to 160  $\mu\text{m}$ , characterizing ESO-H $\alpha$  99 as a YSO in transition from a deeply embedded infrared object (Class I) to a moderately embedded classical T Tauri star. At optical and near-infrared wavelengths, the SED rises steeply, indicating substantial dust obscuration in the line of sight. The integral pre-outburst luminosity of ESO-H $\alpha$  99 from optical wavelengths to the *AKARI* 160  $\mu\text{m}$  data point, a lower limit to the bolometric luminosity since we do not have submillimeter data to complete the SED, is  $34 L_{\odot}$ , adopting again the distance of 1007 pc (B. Pettersson & B. Reipurth 2019, in preparation). This pre-outburst luminosity is high compared to most other T Tauri stars, which are thought to be the precursors of EXor and FUor outbursts, and instead is up in the range of some Herbig Ae/Be stars, specifically the group 2, the flat-spectrum objects as defined by Hillenbrand et al. (1992).

### 3. Observations and Results

We first noted the rise in brightness of ESO-H $\alpha$  99 in data from the ATLAS project, and soon realized that this object had already been noted in *Gaia* (*Gaia* Collaboration et al. 2016) alert Gaia18dvz posted on 2018 December 19 by the Photometric Science Alerts Team<sup>11</sup> with the description “Candidate YSO brightens by more than 1 mag.” The *Gaia* unfiltered (*G* band) photometry covers the years from 2015 to 2019, but has a long gap from 2016 April 27 to 2017 November 2.

#### 3.1. UKIRT Imaging

Deep infrared images were obtained in the *J* and *H* bands with the Wide-Field Camera (WFCAM) described by Casali et al. (2007) on UKIRT in 2019 March and April. The source reached *K<sub>s</sub>*  $\approx 8$  mag near maximum brightness, leading to saturation in the *K* band in the shortest integration times possible with WFCAM on UKIRT. We used the saturated UKIRT *K*-band images primarily to show the reflection nebula in Figure 3. We also used UKIRT for deep imaging in the  $1 - 0 S(1)$  filter to search for shock-excited outflow features

<sup>11</sup> <http://gsaweb.ast.cam.ac.uk/alerts>

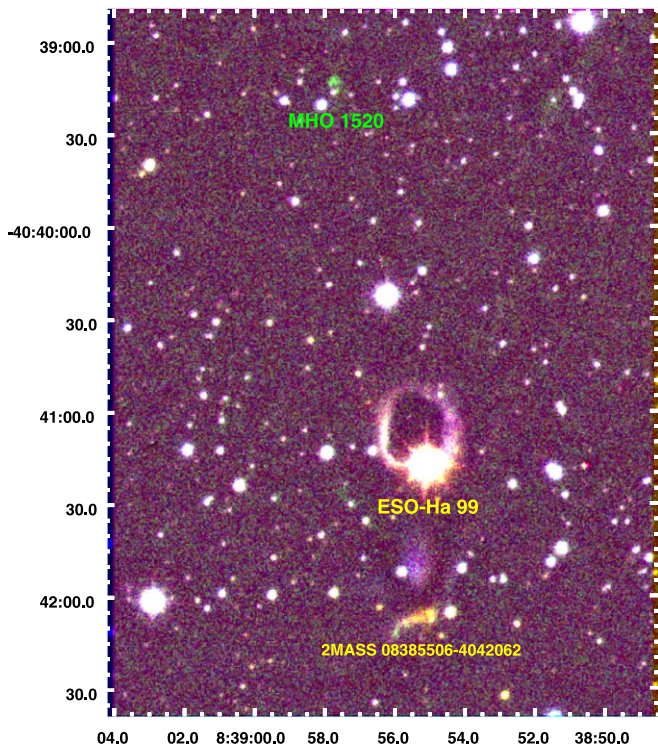


Figure 3. UKIRT color composite of  $H$ ,  $S(1)$ , and  $K$ -band images of ESO  $H\alpha$  99.

and the one emission knot that we found is indicated in Figure 3.

Figure 3 shows a  $H$ ,  $S(1)$ , and  $K$  RGB color composite image obtained with UKIRT. The star ESO- $H\alpha$  99 is associated with a reflection nebula that outlines what appears to be the walls of an outflow cavity. Farther to the north,  $72''$  from the star at P.A.  $14^\circ$ , a single small patch of  $S(1)$  emission with vaguely indicated bow-shock shape, lying roughly on the axis of the reflection nebula, strongly suggests a shock-excited bow shock in a well-collimated outflow. This feature is clearly seen in the UKIRT  $S(1)$  images and was confirmed by  $S(1)$  images with lower resolution from the IRIS telescope. The emission feature is also present on Digital Sky Survey red plates, but not on the B and I plates. An association of this emission feature with ESO- $H\alpha$  99 cannot be conclusively proven without proper motion data, but is strongly suggested based on its morphology and location on the symmetry axis of the reflection nebula. This shock front has now been included in the catalog of Molecular Hydrogen Objects (Davis et al. 2010) as MHO 1520.<sup>12</sup> About  $50''$  to the south of ESO- $H\alpha$  99 a separate reflection nebula and some  $S(1)$  emission associated with the 2MASS source 08385506–4042062 are visible in Figure 3. 2MASS 08385506–4042062 is not visible at optical wavelengths, and is fainter than ESO- $H\alpha$  99 at all wavelengths shown here, indicating relatively low luminosity. It contributes to the flux of the far-infrared source IRAS08370–4030 but is only a minor contribution at any wavelength.

### 3.2. ATLAS

Most of the optical light curve of ESO- $H\alpha$  99 is based on archival data from the ATLAS project described by Tonry et al.

(2018). Photometry in the ATLAS orange ( $O$ ) filter is shown in Figures 4 and 5. ATLAS usually takes more than one image of any given region of the sky in each suitable night to follow fast-moving asteroids. For the light curves in Figures 4 and 5, we have median-combined the individual measurements for each night when the photometric zero-points and sky brightness were stable.

### 3.3. Transiting Exoplanet Survey Satellite Photometry

During its Cycle 1 Sector 8 observations, the *Transiting Exoplanet Survey Satellite* (*TESS*) described by Ricker et al. (2015) observed the ESO- $H\alpha$  99 outburst from 2019 February 2 to 28 with Camera 3. We have reduced these observations using an image subtraction pipeline optimized for *TESS* full-frame images. This pipeline has previously been applied successfully to *TESS* observations of supernovae (Fausnaugh et al. 2019; Vallely et al. 2019) and of the tidal disruption event ASASSN-19bt (Holoien et al. 2019). Because the reference image was constructed from images containing a considerable amount of flux from the EXor, fluxes in the raw difference light curve are systematically lower than their intrinsic values. We correct for this discrepancy by scaling and shifting the differential flux levels to match four ATLAS photometry points obtained concurrently with the *TESS* observations. The *TESS* photometry, as well as these ATLAS observations, are shown in the lower panel of Figure 4. It covered the second interim minimum in the rise of ESO- $H\alpha$  99 to the preliminary brightness maximum.

### 3.4. IRIS, Bochum Monitoring Telescope, and UKIRT

We obtained  $J$ -,  $H$ -, and  $K_s$ -band imaging photometry of ESO- $H\alpha$  99 with the Infrared Imaging System (IRIS) 0.8 m telescope (Hodapp et al. 2010) and the  $1024 \times 1024$   $2.5 \mu\text{m}$  IRIS infrared camera of the Universitätssternwarte Bochum on Cerro Armazones, Chile. In addition to the monitoring with IRIS, we have also obtained deeper images with better spatial resolution obtained in the  $J$  and  $H$  bands with the WFCAM as described above. The WFCAM filters conform to the Mauna Kea Observatory standard described by Tokunaga et al. (2002) and further characterized in Tokunaga & Vacca (2005). Both the UKIRT and IRIS data were calibrated against the 2MASS point-source catalog (Skrutskie et al. 2006) by the Cambridge Astronomical Survey Unit (CASU) using the procedures described by Hodgkin et al. (2009). The source reached  $K_s \approx 8$  mag near maximum brightness, leading to saturation in the  $K$  band in the shortest integration times possible with WFCAM on UKIRT. In  $J$  and  $H$ , both the UKIRT and IRIS photometry were used, while the  $K_s$ -band photometry is only based on IRIS data. The infrared photometry is shown as light curves in Figure 5 and is the basis for the color-color diagram in Figure 6.

Infrared photometry only started in 2019 March after the optical outburst had been noted by ATLAS. The  $J$ ,  $H$ , and  $K_s$  light curve essentially started at the maximum brightness and shows one interim minimum. The total outburst amplitude in the infrared can only be determined in comparison with the Deep Near Infrared Survey of the Southern Sky (DENIS; Epchtein et al. 1997) and 2MASS (Skrutskie et al. 2006) catalog values: DENIS gives the following magnitudes:  $I = 15.938$ ,  $J = 13.063$ ,  $K_s = 9.681$  obtained on JD 2450099.72 and  $I = 15.810$ ,  $J = 13.028$ ,  $K_s = 9.581$  obtained

<sup>12</sup> The MHO catalog is now hosted by D. Froebrich at the University of Kent, UK

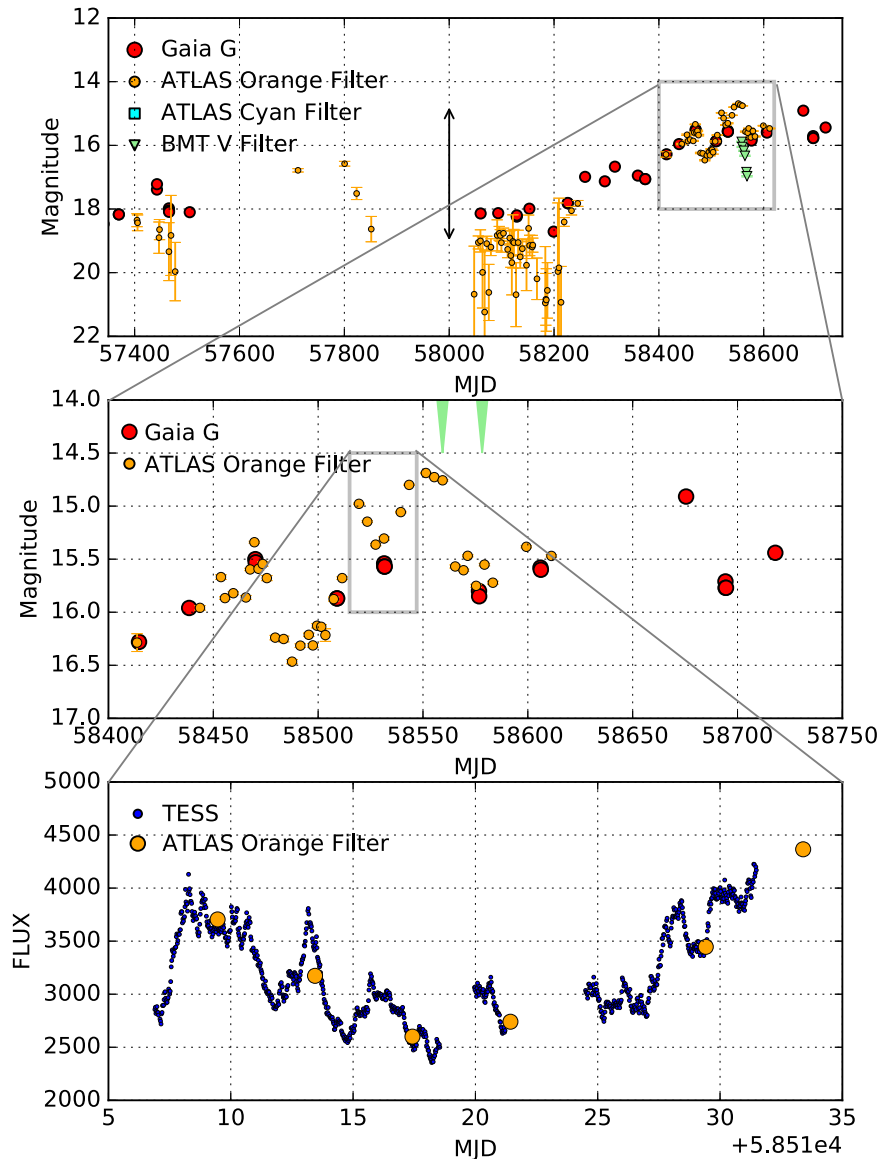


**Figure 4.** Light curve of ESO-H $\alpha$  99 based on archival ATLAS *O* data, *Gaia* archival photometry, and *TESS* photometry. The top panel shows the full light curve from the beginning of the *Gaia* mission. The outburst amplitude in the ATLAS *O* band from the pre-outburst typical magnitude ( $O \approx 19.1$ ) to the maximum of  $O = 14.69$  mag is indicated by an arrow. The middle panel shows the outburst light curve with better resolution. The green arrows indicate the times and light curve points when the two optical spectra (Figures 4 and 7) were obtained. The lower panel shows the *TESS* photometry calibrated against four coinciding ATLAS data points.

on JD 2451207.69 while 2MASS gives  $J = 13.099$ ,  $H = 11.085$ , and  $K_s = 9.414$  obtained on JD 2451236.55. The USNOA2.0 red photographic magnitude is 16.40 (Monet et al. 1998), consistent with our pre-outburst brightness in the ATLAS *O* filter. The DENIS and 2MASS near-infrared pre-outburst magnitudes are consistent with each other, and the two DENIS measurements are consistent over an interval of 1108 days, so we assume that all these measurements represent the quiescent state of ESO-H $\alpha$  99. In Figure 5 the—presumably quiescent—2MASS catalog magnitudes, whose filter band-passes match the IRIS photometry, are indicated by the left-pointing arrows.

We have also obtained *V*-band photometry with the 40 cm Bochum Monitoring Telescope (BMT) on Cerro Armazones (Ramolla et al. 2013), where the object remained observable longer than from Hawaii. The photometry was calibrated against a set of in-field nonvariable stars from the APASS all-

sky catalog (Munari et al. 2014) and are included as green triangle symbols in Figure 4.

### 3.5. Infrared Telescope Facility Infrared and Faulkes Telescope Optical Spectroscopy

Finally, on 2019 March 16, UT, we obtained a near-infrared spectrum of ESO-H $\alpha$  99 using the NASA Infrared Telescope Facility (IRTF) with the SpeX instrument (Rayner et al. 2003) in short cross-dispersed (SXD) mode with a  $0''.3$  slit, giving a spectral resolution of  $R = 2000$ . Low-resolution optical spectra of ESO-H $\alpha$  99 were obtained with the Faulkes Telescope North on Haleakala, Maui, on 2019 March 17 (UT) and 2019 April 5 (UT) using a slit width of  $1''.6$  and  $30''$  slit length of the FLOYDS spectrograph. This resulted in a FWHM of the [O I] night sky lines of  $14 \text{ \AA}$  and a spectral resolution of  $R = 425$  at the wavelength of the Na I doublet.

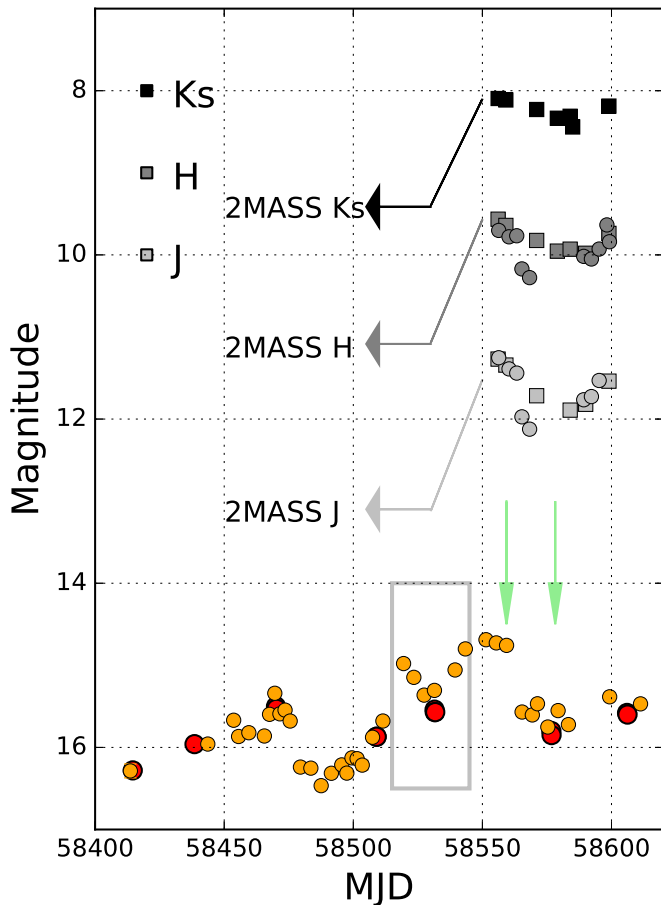


**Figure 5.** Light curve of ESO-H $\alpha$  99 at and after the maximum based on archival ATLAS *C* and *O* data, *Gaia* archival photometry, and post-discovery optical and infrared photometry from BMT, IRIS, and UKIRT described in more detail in the text. The left-pointing arrows indicate the pre-outburst magnitudes from the 2MASS point-source catalog. The green arrows indicate the times and light curve points when the two optical spectra (Figures 7 and 8) were obtained. As in Figure 4, orange circles are ATLAS *O* magnitudes, and red circles are *Gaia* *G* magnitudes.

The optical and infrared spectra from March 17 and 16 (UTC), respectively, were merged into Figure 7. It turned out that these spectra were obtained close to the maximum brightness reached by ESO-H $\alpha$  99 during this outburst.

The spectrum near maximum brightness in Figure 7, combining optical data from the Faulkes telescope and near-infrared data from the IRTF/Spex, shows prominent H I, He I, Ca II, and CO bandhead emission, the only noticeable exception being Na I D line in absorption. Note, however, that Na I is in emission in the near-infrared. Besides the emission lines, a continuum is present, but at the spectral resolution of our data, we cannot detect absorption lines that could be used for spectral classification. The H<sub>2</sub> 1–0 *S*(1) line is weakly detected in emission at the position of the star itself, indicating shock excitation of H<sub>2</sub> near the star.

### 3.6. The Pre-outburst Spectrum

As part of a spectroscopic survey of the brighter stars of the sample of H $\alpha$  emission-line stars in the VMR-D region of Pettersson & Reipurth (1994) a spectrum of ESO-H $\alpha$  99 was obtained on 1993 February 22 at the ESO 3.6 m telescope with the OPTOPUS multi-object spectrograph and an exposure time of  $2 \times 30$  minutes. The original data are no longer available,

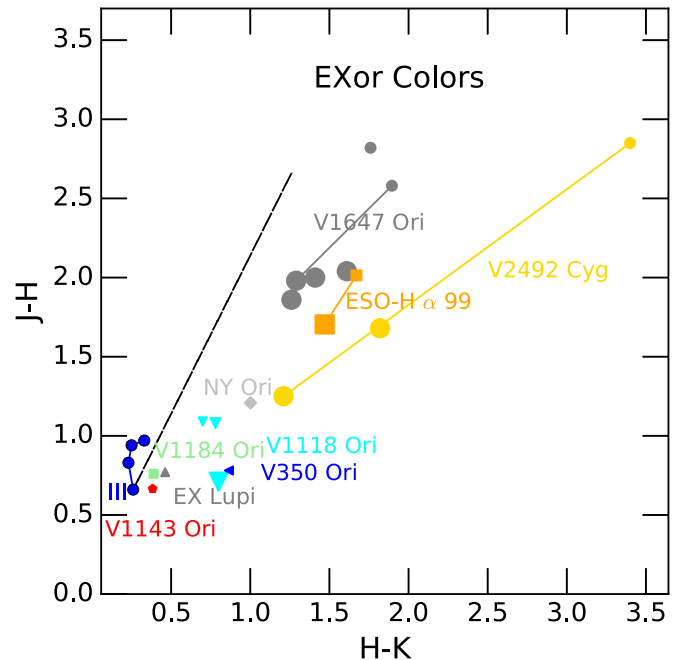


**Figure 6.** Color-color diagram ( $J - H$  vs.  $H - K_s$ ) of ESO-H $\alpha$  99 in quiescence and outburst (orange symbols). Larger symbols represent the bright state of the EXor. For comparison we have included the same known EXors as used in Herbig (2008). We have added additional data on V1647 from Aspin (2011b, and references therein) and data on V1118 Ori from Giannini et al. (2017). The blue filled circles represent the locus of unreddened class III stars from Wegner (2014) and the dashed line represents the reddening vector due to interstellar extinction based on the data by Straižys et al. (2008).

but a plot of the spectrum is. For the analysis in this paper, we have digitized this plot. Although we do not know the photometric brightness of the star at the time this spectrum was taken, we assume that the spectrum represents the quiescent state, as there is no indication of a prior outburst at that time. The pre-outburst spectrum is the one shown in red in the comparison of spectra in Figure 8.

## 4. Discussion

Our goal is to compare the newly discovered and ongoing outburst of ESO-H $\alpha$  99 to well-studied cases and to place it into the context of the ensemble of eruptive events in young stars. In our discussion, we will use the term EXor in the broadest sense describing a young eruptive variable with an emission-line spectrum. Our use of that term is not intended to imply a close similarity of the newly discovered object with specifically the prototype EX Lupi.

### 4.1. Classification of Outburst

The observed outburst amplitude is strongly wavelength dependent, being much larger at optical wavelengths than in the near-infrared. The optical light curve in the ATLAS *O* filter of ESO-H $\alpha$  99 (Figure 4) shows a rise of about 4.4 mag from the quiescent brightness ( $\approx 19.1$  mag) up to the maximum of brightness observed until now ( $O = 14.69$  mag). Just prior to the rise, around MJD 58185, both the ATLAS and *Gaia* data indicate a brief ( $\approx 30$  day) dip in brightness of about 1.3 mag in ATLAS *O* below the quiescent brightness. The immediately following rise in brightness to the maximum is not steady, rather, the ATLAS data show three interim minima superposed on the overall rise of the outburst light curve. As we will

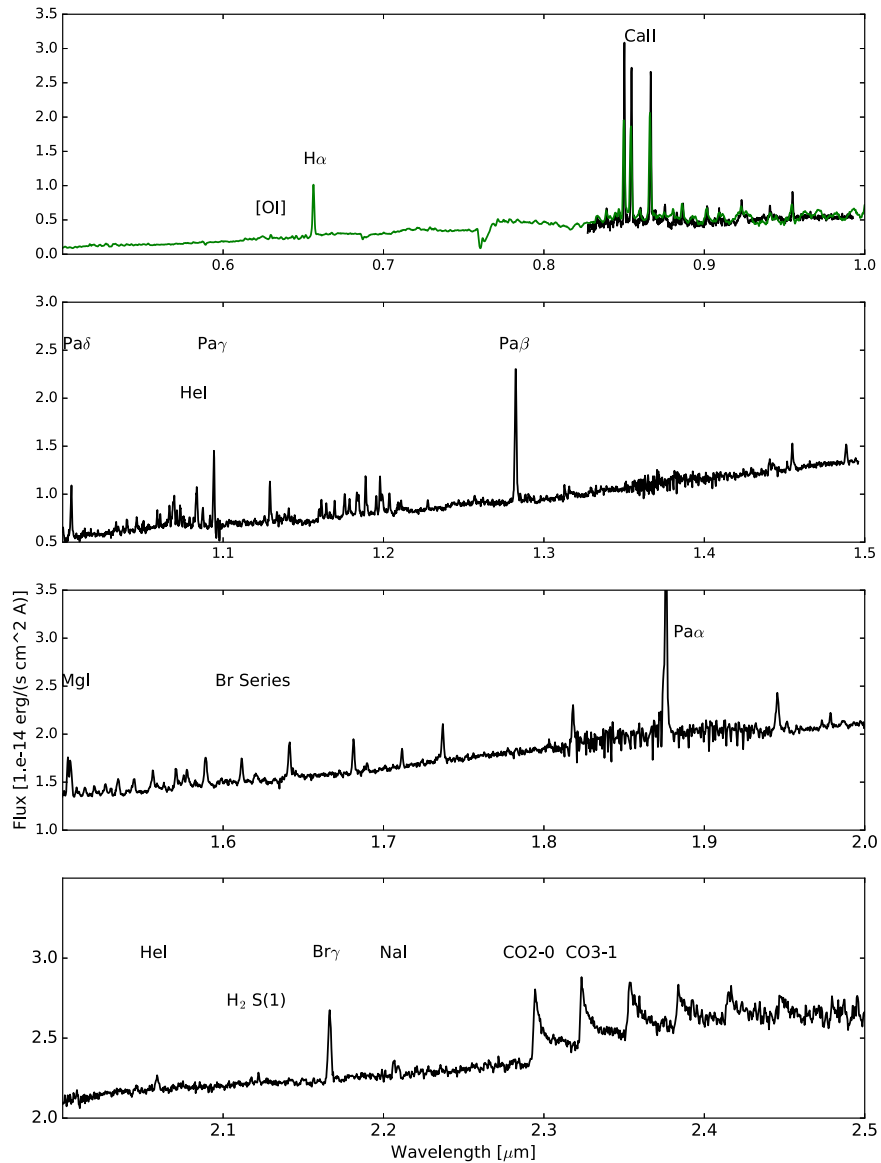


**Figure 7.** IRTF/Spex spectrum from 2019 March 16 UT combined with the optical spectrum (green) taken on 2019 March 17 UT with the FLOYDS spectrograph on the Faulkes Telescope North on Haleakala. The optical spectrum has not been corrected for telluric absorption, while the infrared spectrum has. The spectrum shows strong emission lines, indicating that the outburst is broadly an EXor type.

discuss below in the context of the spectroscopy, at least one of these interim minima in ESO-H $\alpha$  99 is associated with spectral changes. We can exclude that these are merely caused by extinction variations. The few sparse *Gaia* data obtained after ESO-H $\alpha$  99 became observable again in 2019 July and show variations of about 0.5 mag again, similar to the interim minima observed earlier with both the *Gaia* and ATLAS data. We conclude that the semi-periodic fluctuations with typical periods of about one month are continuing now superposed on a fairly stable plateau near maximum brightness.

Quasi-periodicity on the order of one month as observed in ESO-H $\alpha$  99 superposed on the outburst is too long for the expected rotational period of a still rapidly rotating young star and the magnetically coupled accretion flows, but must be related to regions of the rotating disk farther away from the star.

Similar, though shorter period fluctuation superposed on the years-long outburst have been observed by Sicilia-Aguilar et al. (2017) in ASASSN 13db and interpreted as rotational

modulation of starspots that are coming and fading on timescales of months.

About 2 yr before the 2019 major outburst, the ATLAS data indicated a minor maximum around MJD 57800 (2017 February 16). The coverage of this prior maximum by ATLAS is poor, and there are no confirming *Gaia* measurements. We can only state that this maximum lasted for at least a few months, and that the amplitude above the quiescent brightness was about 2.5 mag in the ATLAS *O* filter, substantially less than the present maximum. Despite the limitations of the available data, we note that this smaller prior maximum is entirely consistent with the characteristics of other EXors, as was reviewed in the Section 1, and in particular appears similar to the sporadic outbursts of the prototypical EX Lupi (McLaughlin 1946; Herbig et al. 2001; Herbig 2007), where Aspin et al. (2010) distinguish characteristic and extreme outbursts. In this terminology, the present 2019 outburst of ESO-H $\alpha$  99 qualifies as an extreme outburst, while the smaller 2017 outburst would be characteristic.

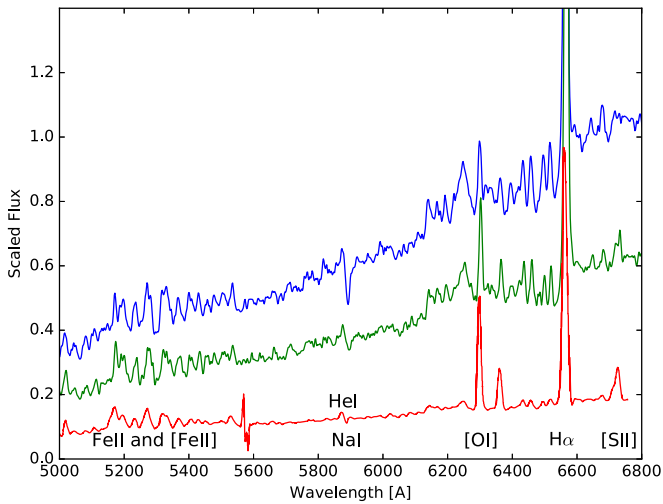


**Figure 8.** Comparison of the optical spectra at three epochs: pre-outburst (1993 February 22, red), maximum brightness (2019 March 17, blue), and declining phase (2019 April 5, green). The spectra are shown qualitatively in the sequence of increasing integrated flux, but are scaled for clarity and not in proportion to the integrated flux. Table 1 gives dates, photometric magnitudes, and relative flux for the three spectra. The timing of the two recent spectra relative to the light curve is indicated by the green arrows in Figures 4 and 5.

#### 4.2. Accretion Instability on Timescales of Days

The outburst of ESO-H $\alpha$  99 was fortuitously observed by *TESS*. The data come from the full-frame images and give photometry on a 30 minute cadence. The resulting finely resolved light curve during the 28 days of observations is shown in the lower panel of Figure 4. The *TESS* observations covered the second of the three minor ( $\approx$ month-long) interim minima superposed on the overall rise to maximum brightness. The *TESS* light curve shows multiple local maxima and minima with typical rise and fall time of the order of one day. A period analysis using the Lomb–Scargle algorithm developed by Lomb (1976) and Scargle (1982), and implemented in the period analysis software (PERANSO) written by T. Vanmunster did not find any strict periodicity of these short-term variations, rather, there is significant power in periods ranging from 2 to 10 days, after whitening out the power associated with the overall minor minimum. These variations on timescales of several days on top of the longer term features of the light curve are similar to the variations during quiescence found by Cody et al. (2017) using *K2* data for YSOs with less substantial disks and bursts (rather than major outbursts) of the order of tens of percent in flux relative to the quiescent, low accretion state.

Variability of FU Ori during its ongoing outburst was studied by Siwak et al. (2013, 2018) and attributed to a small number of unstable accretion tongues (referred to as funnels here) and their associated hotspots, revolving around the star.

Stable accretion funnels and stationary hotspots would lead to rotationally modulated periodic variability on timescales of the rotation of the star, i.e., of the order of a few days. This is not what we observe, however. The short-term variations observed by *TESS* cannot be described as quasi-periodic. At best, they indicate that every few days, something changes. This is best understood if we assume that we observe several active accretion funnels at any given time and their varying accretion rates, coupled with some rotational modulation of this complex scenery.

#### 4.3. Near-infrared Colors and SED

Figure 6 shows the near-infrared  $J - H/H - K$  color-color diagram of ESO-H $\alpha$  99 in both quiescence and outburst. We included similar objects observed by Lorenzetti et al. (2012) and V2492 Cyg, studied in detail by Aspin (2011a) for comparison, as it is the most reddened EXor known to date.

Figure 6 shows that ESO-H $\alpha$  99 shares the colors of the other two deeply embedded EXor objects, V1647 Ori and V2492 Cyg, and shows similar color changes from the quiescent state to the outburst maximum. In general, all EXors get bluer during outburst and the color-color path from quiescent to outburst location is roughly parallel to the interstellar reddening vector, if anything slightly less steep. While the color changes are therefore consistent with a clearing of obscuring material during outburst, this is certainly not the only mechanism at work in ESO-H $\alpha$  99 since we are also seeing major changes in the line ratios in the spectrum. Those spectral changes cannot be explained simply by a varying amount of line-of-sight extinction. Some contribution from changing extinction, possibly caused by irregularities in the inner disk orbiting in and out of the line of sight is quite possible, but cannot be confirmed with the available data.

We have compared the pre-outburst SED of ESO-H $\alpha$  99 (Figure 2) with the SEDs of other EXors and FUors using the VizieR database and its photometry viewer. This database is readily available, so we do not show all SEDs here. The wavelength coverage of those SEDs is quite heterogeneous, so we will not discuss the similarities and differences quantitatively. The SEDs of most classical, i.e., low extinction EXors, some of which are included in the near-infrared color-color diagram in Figure 6 and occupy the low-color-value area of this diagram, have the peak of their SED at near-infrared wavelengths, and decline from there to the long-wavelength limit of the available data. Only the deeply embedded EXors show flat or nearly flat SEDs; NY Ori is flat from 1 to 20  $\mu\text{m}$ , but has no data beyond that. Deeply embedded, very red EXors such as V2492 Cyg, PV Cep, and V1647 Ori have essentially flat SEDs out to 100  $\mu\text{m}$ . The SED of ESO-H $\alpha$  99 is very similar to those three deeply embedded flat SED EXors. This flat 10–100  $\mu\text{m}$  SED also puts ESO-H $\alpha$  99 in the same SED class as OO Ser, the deeply embedded outburst star (Hodapp et al. 1996) that falls outside of the classical FUor versus EXor classification scheme.

We also note that the classical FUors FU Ori and V1057 Cyg have SED peaks at near-infrared wavelengths. The FUor V2775 Ori, however, (Fischer et al. 2012) has a flat SED similar to the one discussed here. Deeply embedded FUor-like objects, i.e., objects spectroscopically similar to a FUor but with no historically observed outburst, such as L1551 IRS5, have SEDs rising throughout the 10–100  $\mu\text{m}$  range.

While EX Lupi, the prototypical EXor, is not associated with much nebulosity and is not deeply embedded, ESO-H $\alpha$  99 is highly reddened and is associated with a reflection nebula with a bubble-like morphology, probably light scattered off the walls of an outflow cavity. Both its red colors and the presence of a reflection nebula support the fact that ESO-H $\alpha$  99 is a very young object, still deeply embedded in its parent molecular cloud, and surrounded by a substantial gas and dust disk. We have found one small region of shock-excited H $_2$  1 – 0 S(1) emission with indication of a bow-shock morphology near the symmetry axis of the reflection nebula, strongly suggesting that this feature is the result of a highly collimated outflow from

**Table 1**  
Optical Spectroscopy

	1993 Feb 22	2019 Mar 17	2019 Apr 5
Magnitude ( $O$ )	$\sim 19$	14.76	15.55
Rel. flux	0.02	1.00	0.48
Color in Figure 8	Red	Blue	Green
[O I] 6300 EW ( $\text{\AA}$ )	-29.3	-2.2	-4.7
[O I] 6364 EW ( $\text{\AA}$ )	-11.5	low S/N	-1.4
H I 6563 EW ( $\text{\AA}$ )	-75.1	-36.5	-58.9
[S II] 6716+6731 EW ( $\text{\AA}$ )	-19.4	-0.9	-1.8
Ca II 8498 EW ( $\text{\AA}$ )	No data	-35.0	-47.7
Ca II 8542 EW ( $\text{\AA}$ )	No data	-37.2	-52.2
Ca II 8662 EW ( $\text{\AA}$ )	No data	-41.9	-54.0

ESO-H $\alpha$  99. Such highly collimated outflows are frequently found in YSOs, but are not typical of EXors or FUors. We interpret this as additional evidence that ESO-H $\alpha$  99 is, within the broad EXor class of outbursts, one of the youngest of this class of objects.

#### 4.4. Spectral Changes during Outburst

We compare low-resolution optical spectra of ESO-H $\alpha$  99 at three epochs: the pre-outburst spectrum from 1993 February 22, presumably during a quiescent phase, the spectrum taken very close to the maximum of the current outburst on 2019 March 17 shown in Figure 7, and the spectrum taken on 2019 April 5 when the ATLAS  $O$  magnitude was 0.8 mag lower than at the maximum.

We do not have coincident photometry for the pre-outburst spectrum from 1993 February 22. From Figure 4 it is clear that ESO-H $\alpha$  99 had shown some variability prior to the present outburst. On the other hand, none of the pre-outburst data (Palomar Observatory Sky Survey, 2MASS, etc.) give any indication of a prior large outburst. Our measured quiescent pre-outburst brightness in the ATLAS orange filter is about  $O = 19.1$  mag. We therefore make the assumption that at the time of the 1993 spectrum, the brightness was  $O \approx 19$  mag.

For the two epochs in 2019, we have closely coincident ATLAS orange filter photometry. For 2019 March 17, ATLAS obtained photometry in the same night, about 1.25 hr after the spectrum. For the 2019 April 5 spectrum, the closest ATLAS photometry is from the following night, 25.7 hr after the spectrum. The epochs of the recent spectra are indicated by the blue arrows in Figures 4 and 5 and place those spectra in context of the light curve. Of the two 2019 optical spectra, the first was obtained near the maximum of the observed light curve during this ongoing outburst, and the second in the following minor interim minimum in the light curve, after which the object brightened again. In the middle panel of Figure 4 and in Figure 5, the brightness maximum at the time of the first spectrum and the interim minimum on 2019 April 5 are documented by ATLAS  $O$ , and infrared  $J$ ,  $H$ , and  $K$  photometry. Table 1 lists the dates, ATLAS  $O$  magnitudes, and the equivalent width of four spectral lines, both permitted and forbidden.

For now, we can leave the question open whether March 17 marked the overall maximum on the current outburst, or whether it is merely a preliminary interim maximum. After it reemerged from behind the Sun in 2019 August, we have obtained a few new *Gaia* data points indicating that ESO-H $\alpha$  99 has experienced another high point near the magnitude of

the 2019 March maximum and is otherwise staying within a magnitude of the maximum brightness with some variations. The important point is that changes in broadband photometry are associated with changes in the emission-line spectrum.

The early 1993 optical spectrum of ESO-H $\alpha$  99 offers some insight into what we assume is the quiescent state of the star: First, the 26 yr old spectrum shows the forbidden lines of [O I] at 6300 and 6363  $\text{\AA}$  and blended [S II] 6716/6731  $\text{\AA}$ , which together with strong H $\alpha$  emission are characteristic of Herbig–Haro shocks. The molecular hydrogen shock front MHO 1520 approximately along the line defined by the outflow cavity associated with ESO-H $\alpha$  99 (Figure 3) shows that outflow activity must have occurred in the more distant past, certainly prior to the present outburst.

Second, a forest of permitted Fe II and forbidden [Fe II] lines is seen in the 5000–5500  $\text{\AA}$  region. These lines are only seen in the most active T Tauri stars (Herbig 1962), and the spectrum shows a strong semblance to that of the HH 32 driving source AS 353A (Eisloffel et al. 1990) and the HH 46/47 driving source (Reipurth & Heathcote 1991).

Third, the Na I doublet at  $\lambda 5890/5896$   $\text{\AA}$  is in absorption, fairly weak, and unresolved in the 1993 spectrum as well as in the 2019 spectra. The Na I absorption blends with the He I line at 5876  $\text{\AA}$ . Helium emission lines have been observed in several other EXors, e.g., NY Ori, V1118 Ori, and V350 Ori by Herbig (2008).

Altogether, the 1993 quiescent spectrum is indicative of a highly active, strongly accreting YSO star that is driving a shocked outflow.

During the present outburst, the spectrum has changed substantially. Referring to Table 1, the equivalent width of all the emission lines was much higher in quiescence (1993) than during the outburst. The H $\alpha$  line was much higher ( $\sim 75$   $\text{\AA}$ ) than in the 2019 March 17 spectrum ( $\sim 37$   $\text{\AA}$ ). On 2019 April 5, at a time when the broadband integrated flux was only about one-half of that at maximum, the spectrum has an H $\alpha$  equivalent width between those two extreme points: EW  $\sim 62$   $\text{\AA}$ .

The spectral changes observed between those two 2019 spectra clearly indicate that this interim minimum was not just caused by changing amounts of obscuring dust in the line of sight, which should not affect the equivalent width of H $\alpha$ . Rather, the photometric and spectral variations show real changes in the components of the accretion flow: inner disk, accretion funnels, and possibly a surface hot spot on the star.

Comparing the change of H $\alpha$  equivalent width to the change in broadband flux in Table 1, it is clear that the flux of the H $\alpha$  line does increase with increasing brightness, but that the continuum rises disproportionately more strongly, so that the equivalent width is reduced by about a factor of two between quiescence and the brightness maximum. Similarly, for the two recent epochs that we have a measured brightness for, the H $\alpha$  equivalent width increases by a factor of 1.6 during a decline on a factor 0.48 in broadband brightness, showing again that the continuum changes disproportionately more than the H $\alpha$  line flux.

The disproportionate rise of the continuum is even more pronounced for the forbidden lines, the brightest of which is [O I] at 6300  $\text{\AA}$ . From quiescence to the maximum, a factor of  $\approx 50$  in broadband flux, the equivalent width is reduced by a factor of  $\approx 13$ . So while the line flux in [O I] 6300  $\text{\AA}$  does increase somewhat during maximum, the broadband flux

increases 13 times more, showing that during maximum, the conditions are less favorable for the emission of forbidden lines, probably because of higher densities in the emitting regions. Given the uncertainty of our assumption for the pre-outburst brightness when the 1993 February 22 spectrum was taken, the ESO-H $\alpha$  99 spectral evolution is consistent with the flux in those forbidden lines being unchanged during the outburst, and simply being diluted by increased continuum or that line flux increasing by much less than the continuum. Comparing just the 2019 March 17 (maximum) and 2019 April 5 (post-maximum) equivalent widths of [O I]6300 Å and the blended [S II] lines, we clearly note that the equivalent width changes inversely proportional to the broadband flux, i.e., the absolute line flux stays constant. The accretion sensitive (Muzerolle et al. 1998) permitted Ca II triplet lines show an increase of a factor 1.3 during the decline by a factor of 0.48, meaning that the absolute line flux has diminished, but not proportional to the continuum flux.

We are now comparing the spectral evolution of ESO-H $\alpha$  99 with several other EXor objects and one higher luminosity eruptive variable. The optical spectrum of ESO-H $\alpha$  99 and its changes during the outburst are quite different from those observed in the 2008 outburst of the prototypical EX Lupi. Kospal et al. (2008) and Sicilia-Aguilar et al. (2012, 2015) observed a very rich emission-line spectrum, compared to other T Tauri stars, and a substantial increase in the number of metal emission lines during outburst, more than most other EXor-type outbursts, but note the absence of forbidden lines. As a caveat to the latter statement, in high resolution spectra, the emission of [O I] was detected in EX Lupi by Banzatti et al. (2019) both in quiescence and, more strongly, during the 2008 outburst.

Similarly, Holoien et al. (2014, p. 37) observed in the case of the 2013 EXor eruption of ASASSN13db that “during the outburst, the spectra are dominated by a forest of emission lines, mostly neutral metallic lines from Fe I.” The longer duration 2014–2017 outburst of this object was studied by Sicilia-Aguilar et al. (2017) and they note again the similarity of the outburst spectrum to that of EX Lupi.

The spectral changes in these two objects are clearly different from the eruption of ESO-H $\alpha$  99 where we observe a reduction in the prominence of the Fe I line forest, and a substantial reduction in the equivalent width, i.e., the importance relative to the continuum, for the forbidden lines of [O I] and [S II].

In contrast, the evolution of the spectral lines during the outburst of ESO-H $\alpha$  99 has more similarities to the higher luminosity case PV Cep. Kun et al. (2011) found nearly constant flux, i.e., strongly increasing equivalent widths, in forbidden lines during the fading. However, they also noted little change in the equivalent width of H $\alpha$  in the fading phase, which is different from what we observe in ESO-H $\alpha$  99.

We conclude that during the ESO-H $\alpha$  99 outburst, its spectrum has changed substantially. The H $\alpha$  line changes less than the continuum during the outburst, and the forbidden [O I] and [S II] lines change substantially less than the continuum, and are, in fact, consistent with these forbidden line fluxes being constant.

We conclude that in ESO-H $\alpha$  99, the region emitting the forbidden lines may not be affected at all by the processes leading to the continuum outburst. The increase in the optical and near-infrared continuum is qualitatively similar to the

appearance of a strong continuum during FUor outbursts. We speculate that in ESO-H $\alpha$  99, the rise in the continuum is less than in typical FUor outbursts, leaving the most prominent emission lines observable.

## 5. Summary and Conclusions

The optical (ATLAS *O*) light curve of ESO-H $\alpha$  99 shows a rise of about 4.4 mag from the pre-outburst average. We also have indications for a previous small maximum of 2.5 mag amplitude in 2016, and for a brief dip in brightness by 1.3 mag just prior to the rise of the present maximum. The high-cadence *TESS* light curve during a minor interim dip in brightness just prior to reaching maximum light shows fluctuations of the order of 10% in flux and typical durations of a few days, but without clear periodicity.

ESO-H $\alpha$  99 is associated with an optical and near-infrared reflection nebula. There is one knot of line emission (MHO 1520) found in the H $_2$  1 – 0 *S*(1) emission line, but also indicated in the optical *R* band. This is most likely a Herbig–Haro object associated with collimated outflow activity. The H $_2$  1–0 *S*(1) emission line is also seen at the position of the star.

ESO-H $\alpha$  99 shares the near-infrared colors and mid-to-far-infrared SED of the most deeply embedded EXors. ESO-H $\alpha$  99 is a YSO of fairly high quiescent luminosity (34  $L_{\odot}$ ), much higher than typical EXors, and may be an intermediate mass star.

Two spectra during the present outburst show many emission lines, in particular H $\alpha$ , Ca II, and CO bandhead emission, making ESO-H $\alpha$  99 spectroscopically similar to other deeply embedded EXor outbursts. Comparison with a pre-outburst spectrum from 1993 shows, however, that several emission lines that had been present during quiescence are partly diluted by continuum emission. The H $\alpha$  equivalent width is largest in quiescence, smallest near the light curve maximum, and intermediate a few weeks after the maximum. The rise in overall brightness during this EXor event is largely due to the disproportionate rise of the continuum compared to the emission lines. This effect is particularly strong for the forbidden [O I] and [S II] lines. If the light curve does indeed show the typical evolution of an EXor, the next observing season in late 2019 may show the decline of brightness back to the pre-outburst level.

This work has made use of data from the European Space Agency (ESA) mission *Gaia*<sup>13</sup> and processed by the *Gaia* Data Processing and Analysis Consortium (DPAC).<sup>14</sup> Funding for the DPAC has been provided by national institutions, in particular the institutions participating in the *Gaia* Multilateral Agreement. ATLAS observations and this work were supported by NASA grant NN12AR55G. The AAVSO Photometric All-Sky Survey (APASS) was funded by the Robert Martin Ayers Sciences Fund. Infrared photometric data on ESO-H $\alpha$  99 were obtained at the IRIS telescope of the Universitätssternwarte Bochum on Cerro Armazones, which is operated under a cooperative agreement between the “Astronomisches Institut, Ruhr Universität Bochum,” Germany, and the Institute for Astronomy, University of Hawaii, USA. Construction of the IRIS infrared camera was supported by the National Science Foundation under grant AST07-04954. This

<sup>13</sup> <https://www.cosmos.esa.int/gaia>

<sup>14</sup> <https://www.cosmos.esa.int/web/gaia/dpac/consortium>

work makes use of observations from the LCOGT network. This paper uses data collected under the ESO/RUB USB agreement at the Paranal Observatory. This paper includes data collected by the *TESS* mission. Funding for the *TESS* mission is provided by the NASA Explorer Program. This work is based in part on archival data obtained with the *Spitzer Space Telescope*, which is operated by the Jet Propulsion Laboratory, California Institute of Technology under a contract with NASA, and on archival data from *AKARI*, a JAXA project with the participation of ESA. The infrared spectrum was obtained with the SpeX instrument at the Infrared Telescope Facility, which is operated by the University of Hawaii under contract NNH14CK55B with the National Aeronautics and Space Administration. Near-infrared imaging data from the WFCAM at the UKIRT observatory operated by the University of Hawaii were used in this paper. P.J.V. is supported by the National Science Foundation Graduate Research Fellowship Program Under grant No. DGE-1343012. C.S.K. is supported by NSF grants AST-1515876, AST-1515927, and AST-181440. This work made use of the ADS, Simbad, and VieziR. We wish to thank the referee for constructive comments that helped improve this paper.

*Facilities:* ATLAS, FTN, *Gaia*, OCA:IRIS, IRTF, *TESS*, UKIRT.

### ORCID iDs

Klaus W. Hodapp  <https://orcid.org/0000-0003-0786-2140>

Bo Reipurth  <https://orcid.org/0000-0001-8174-1932>

John Tonry  <https://orcid.org/0000-0003-2858-9657>

Benjamin J. Shappee  <https://orcid.org/0000-0003-4631-1149>

C. S. Kochanek  <https://orcid.org/0000-0001-6017-2961>

Michael Fausnaugh  <https://orcid.org/0000-0002-9113-7162>

### References

- Abrahamyan, H. V., Mickaelian, A. M., & Knyazyan, A. V. 2015, *A&C*, **10**, 99
- Aspin, C. 2011a, *AJ*, **141**, 196
- Aspin, C. 2011b, *AJ*, **142**, 135
- Aspin, C., Barbieri, C., Boschi, F., et al. 2006, *AJ*, **132**, 1298
- Aspin, C., Beck, T. L., & Reipurth, B. 2008, *AJ*, **135**, 423
- Aspin, C., Greene, T. P., & Reipurth, B. 2009, *AJ*, **137**, 2968
- Aspin, C., & Reipurth, B. 2009, *AJ*, **138**, 1137
- Aspin, C., Reipurth, B., Beck, T. L., et al. 2009, *ApJL*, **692**, L67
- Aspin, C., Reipurth, B., Herczeg, G. J., & Capak, P. 2010, *ApJL*, **719**, L50
- Aspin, C., & Sandell, G. 1994, *A&A*, **288**, 803
- Audard, M., Ábrahám, P., Dunham, M. M., et al. 2014, in *Protostars and Planets VI*, ed. H. Beuther, R. S. Klessen, C. P. Dullemond, & T. Henning (Tucson, AZ: Univ. Arizona Press), 387
- Banzatti, A., Pascucci, I., Edwards, S., et al. 2019, *ApJ*, **870**, 76
- Casali, M., Adamson, A., Alves de Oliveira, C., et al. 2007, *A&A*, **467**, 777
- Cody, A. M., Hillenbrand, L. A., David, T. J., et al. 2017, *ApJ*, **836**, 41
- Cody, A. M., Stauffer, J., Baglin, A., et al. 2014, *AJ*, **147**, 82
- Contreras Peña, C., Lucas, P. W., Kurtsev, R., et al. 2017a, *MNRAS*, **465**, 3039
- Contreras Peña, C., Lucas, P. W., Minniti, D., et al. 2017b, *MNRAS*, **465**, 3011
- Dame, T. M., Ungerechts, H., Cohen, R. S., et al. 1987, *ApJ*, **322**, 706
- Davis, C. J., Gell, R., Khanzadyan, T., Smith, M. D., & Jenness, T. 2010, *A&A*, **511**, A24
- Eisloffel, J., Guenther, E., Hessman, F. V., et al. 1991, *ApJL*, **383**, L19
- Eisloffel, J., Solf, J., & Boehm, K. H. 1990, *A&A*, **237**, 369
- Epchtein, N., de Batz, B., Capoani, L., et al. 1997, *Msngr*, **87**, 27
- Fausnaugh, M. M., Valley, P. J., Kochanek, C. S., et al. 2019, arXiv:1904.02171
- Fischer, W. J., Megeath, S. T., Tobin, J. J., et al. 2012, *ApJ*, **756**, 99
- Gaia Collaboration, Brown, A. G. A., Vallenari, A., et al. 2016, *A&A*, **595**, A2
- Gaia Collaboration, Brown, A. G. A., Vallenari, A., et al. 2018, *A&A*, **616**, A1
- Gaia Collaboration, Prusti, T., de Bruijne, J. H. J., et al. 2016, *A&A*, **595**, A1
- Giannini, T., Antonucci, S., Lorenzetti, D., et al. 2017, *ApJ*, **839**, 112
- Giannini, T., Lorenzetti, D., De Luca, M., et al. 2007, *ApJ*, **671**, 470
- Greene, T. P., Wilking, B. A., Andre, P., et al. 1994, *ApJ*, **434**, 614
- Hartmann, L., Herczeg, G., & Calvet, N. 2016, *ARA&A*, **54**, 135
- Herbig, G. H. 1962, *AdA&A*, **1**, 47
- Herbig, G. H. 1977, *ApJ*, **217**, 693
- Herbig, G. H. 2007, *AJ*, **133**, 2679
- Herbig, G. H. 2008, *AJ*, **135**, 637
- Herbig, G. H., Aspin, C., Gilmore, A. C., Imhoff, C. L., & Jones, A. F. 2001, *PASP*, **113**, 1547
- Hillenbrand, L. A., Miller, A. A., Carpenter, J. M., et al. 2019, *ApJ*, **874**, 82
- Hillenbrand, L. A., Strom, S. E., Vrba, F. J., et al. 1992, *ApJ*, **397**, 613
- Hodapp, K. W., & Chini, R. 2014, *ApJ*, **794**, 169
- Hodapp, K. W., Chini, R., Reipurth, B., et al. 2010, *Proc. SPIE*, **7735**, 77351A
- Hodapp, K. W., Chini, R., Watermann, R., & Lemke, R. 2012, *ApJ*, **744**, 56
- Hodapp, K.-W., Hora, J. L., Rayner, J. T., Pickles, A. J., & Ladd, E. F. 1996, *ApJ*, **468**, 861
- Hodgkin, S. T., Irwin, M. J., Hewett, P. C., et al. 2009, *MNRAS*, **394**, 675
- Holoien, T. W.-S., Prieto, J. L., Stanek, K. Z., et al. 2014, *ApJL*, **785**, L35
- Holoien, T. W.-S., Valley, P. J., Auchettl, K., et al. 2019, *ApJ*, **883**, 111
- Kospal, A., Nemeth, P., Abraham, P., et al. 2008, *IBVS*, **5819**, 1
- Kun, M., Szegedi-Elek, E., Moór, A., et al. 2011, *MNRAS*, **413**, 2689
- Lasker, B. M., Lattanzi, M. G., McLean, B. J., et al. 2008, *AJ*, **136**, 735
- Liseau, R., Lorenzetti, D., Nisini, B., et al. 1992, *A&A*, **265**, 577
- Lomb, N. R. 1976, *Ap&SS*, **39**, 447
- Lorenzetti, D., Antonucci, S., Giannini, T., et al. 2012, *ApJ*, **749**, 188
- Lorenzetti, D., Giannini, T., Antonucci, S., et al. 2015, *ATel*, **7935**, 1
- Lorenzetti, D., Giannini, T., Larionov, V. M., et al. 2011, *ApJ*, **732**, 69
- Massi, F., De Luca, M., Elia, D., et al. 2007, *A&A*, **466**, 1013
- May, J., Murphy, D. C., & Thaddeus, P. 1988, *A&AS*, **73**, 51
- McLaughlin, D. B. 1946, *AJ*, **52**, 109
- Monet, D. G. 1998, USNO-A2.0 (Flagstaff, AZ: US Nav. Obs)
- Munari, U., Henden, A., Frigo, A., et al. 2014, *AJ*, **148**, 81
- Murphy, D. C., & May, J. 1991, *A&A*, **247**, 202
- Muzerolle, J., Hartmann, L., & Calvet, N. 1998, *AJ*, **116**, 455
- Pettersson, B. 2008, in *Handbook of Star-forming Regions*, Vol. II, ed. B. Reipurth (San Francisco: ASP), 43
- Pettersson, B., & Reipurth, B. 1994, *A&AS*, **104**, 233
- Prisinzano, L., Damian, F., Guarcello, M. G., et al. 2018, *A&A*, **617**, A63
- Ramolla, M., Drass, H., Lemke, R., et al. 2013, *AN*, **334**, 1115
- Rayner, J. T., Toomey, D. W., Onaka, P. M., et al. 2003, *PASP*, **115**, 362
- Reipurth, B., & Aspin, C. 2004, *ApJL*, **606**, L119
- Reipurth, B., & Heathcote, S. 1991, *A&A*, **246**, 511
- Ricker, G. R., Winn, J. N., Vanderspek, R., et al. 2015, *JATIS*, **1**, 14003
- Rodgers, A. W., Campbell, C. T., & Whiteoak, J. B. 1960, *MNRAS*, **121**, 103
- Sandqvist, A., & Lindroos, K. P. 1976, *A&A*, **53**, 179
- Scargle, J. D. 1982, *ApJ*, **263**, 835
- Sicilia-Aguilar, A., Fang, M., Roccatagliata, V., et al. 2015, *A&A*, **580**, A82
- Sicilia-Aguilar, A., Oprandi, A., Froebrich, D., et al. 2017, *A&A*, **607**, A127
- Sicilia-Aguilar, A., Kóspál, Á., Setiawan, J., et al. 2012, *A&A*, **544**, A93
- Siwak, M., Rucinski, S. M., Matthews, J. M., et al. 2013, *MNRAS*, **432**, 194
- Siwak, M., Winiarski, M., Ogłóza, W., et al. 2018, *A&A*, **618**, A79
- Skrutskie, M. F., Cutri, R. M., Stiening, R., et al. 2006, *AJ*, **131**, 1163
- Stauffer, J., Cody, A. M., Baglin, A., et al. 2014, *AJ*, **147**, 83
- Strafella, F., Elia, D., Campeggio, L., et al. 2010, *ApJ*, **719**, 9
- Strafella, F., Lorenzetti, D., Giannini, T., et al. 2015, *ApJ*, **798**, A104
- Straizys, V., Corbally, C. J., & Laugalys, V. 2008, *BaltA*, **17**, 125
- Tokunaga, A. T., Simons, D. A., & Vacca, W. D. 2002, *PASP*, **114**, 792
- Tokunaga, A. T., & Vacca, W. D. 2005, *PASP*, **117**, 421
- Tonry, J. L., Denneau, L., Heinze, A. N., et al. 2018, *PASP*, **130**, 064505
- Valley, P. J., Fausnaugh, M., Jha, S. W., et al. 2019, *MNRAS*, **487**, 1385
- Wegner, W. 2014, *AcA*, **64**, 261
- Yamaguchi, N., Mizuno, N., Saito, H., et al. 1999, *PASJ*, **51**, 775